nature geoscience

ARTICLES

https://doi.org/10.1038/s41561-022-00913-6

Asymmetry in the seasonal cycle of Antarctic sea ice driven by insolation

L. A. Roach[1,5,6], I. Eisenman[2]✉, T. J. W. Wagner[3,4], E. Blanchard-Wrigglesworth[1] and C. M. Bitz[1]

The mean seasonal cycle of Antarctic sea-ice extent is asymmetric, with the period of ice retreat being approximately two months shorter than the period of ice advance. This feature is largely consistent in observations from year to year and across different satellite products. The asymmetry is also broadly reproduced by comprehensive climate models across generations from CMIP3 to CMIP6, with limited impacts from internal variability. Using a range of idealized climate models of varying complexity, we show that the seasonal cycle in top-of-atmosphere incident solar radiation drives the asymmetry. Because insolation in southern high latitudes departs from a sinusoid by having a narrow peak of intense brightness in summer and a long period of low light in winter, there is rapid summer ice retreat and gradual winter ice advance. This simple physical explanation is markedly different from those proposed in previous studies.

The seasonal growth and melt of Antarctic sea ice represents one of the largest annual surface cover changes on Earth. Antarctic sea ice is a key driver of the upper ocean freshwater budget[1] and the formation of Antarctic Bottom Water[2], which is a main component of the global ocean circulation. Changes in the sea-ice cover can have impacts on the Antarctic Ice Sheet[3]; Antarctic sea ice also plays a role in marine ecosystems and primary production[4]. The phase delay of sea ice relative to insolation influences the fraction of sunlight reflected annually back to space, a key component of Earth's energy budget.

There is a striking asymmetry in the seasonal cycle of Antarctic sea-ice extent between fast decay during ~5 months of the year and slow growth during the remaining ~7 months (ref. [5]). This is not mirrored in the Arctic, where the durations of sea-ice retreat and advance are more similar (Supplementary Fig. 1). Much previous work has attempted to explain the enigma of this seasonal asymmetry in Antarctic sea-ice extent (see ref. [5] for a recent review). One of the main mechanisms put forward previously, based on an energy budget analysis from observations, is that upwelling and associated warm surface waters accelerate sea-ice melt[6,7]. An alternative mechanism, based on connections identified in observations, has the asymmetry caused by processes in the atmosphere rather than the ocean, with the semi-annual oscillation of the atmospheric low-pressure trough that surrounds the Antarctic continent creating patterns of convergence and divergence of Antarctic sea ice that favour fast ice retreat[8–12]. In this article, we systematically investigate the physical mechanism responsible for this asymmetry using observations and a range of climate models.

Observations and comprehensive climate models

The observed mean seasonal cycle in Antarctic sea-ice extent is plotted in Fig. 1 (see Methods for details). The seasonal asymmetry can be readily seen in the plot. As a measure of this asymmetry, we define δ_l as the difference in length between the ice advance and retreat periods, with positive values indicating a shorter retreat season. In other words, δ_l is the duration of the advance season (that is, time from minimum to maximum ice extent) minus the duration of the retreat season (that is, time from maximum to minimum). In Fig. 1, the summer minimum occurs on 24 February, and the winter maximum occurs on 20 September. This implies that the retreat period is 51 days shorter than the growth period: $\delta_l = 51$ days for the mean seasonal cycle. This value is broadly consistent from year to year, across satellite data products and for both sea-ice extent and sea-ice area (Supplementary Figs. 1b and 2).

Next we examine the Antarctic sea ice seasonal cycle simulated by the current generation of comprehensive climate models, using output from the Coupled Model Intercomparison Project Phase 6 (CMIP6). The simulated values of δ_l for each model are shown in Fig. 2. The multimodel mean value is $\delta_l = 53 \pm 13$ days, with the error bar representing one standard deviation among the models. This agreement with the observations is striking given the substantial documented model biases in Antarctic sea-ice climatology, variability and trends[13–18]. We find that the preceding generation of models (CMIP5) also broadly captures the asymmetry in Antarctic sea ice, although with slightly more intermodel spread than CMIP6 (Supplementary Fig. 3a,c). A qualitatively similar asymmetry also occurs in the earlier CMIP3 models (Supplementary Fig. 4a), although only monthly data are available, which makes the diagnosis of seasonal asymmetry less accurate (see Methods for details).

Hence, comprehensive climate models robustly capture the observed asymmetry in Antarctic sea ice, even in CMIP3 models, which are less complex than later generations. This implies that the asymmetry occurs due to physical processes that are accurately captured across the range of climate models, despite myriad differences among the individual models. Based on this, we next turn to an idealized climate model that includes representations of only a small set of fundamental processes.

Idealized climate model

We adapt an idealized model of sea ice and climate that was developed previously by ref. [19] (hereafter WE15). It is a diffusive

[1]Atmospheric Sciences, University of Washington, Seattle, WA, USA. [2]Scripps Institution of Oceanography, University of California, San Diego, CA, USA. [3]Atmospheric and Oceanic Sciences, University of Wisconsin, Madison, WI, USA. [4]Physics and Physical Oceanography, University of North Carolina, Wilmington, NC, USA. [5]Present address: NASA Goddard Institute for Space Studies, New York, NY, USA. [6]Present address: Center for Climate Systems Research, Columbia University, New York, NY, USA. ✉e-mail: eisenman@ucsd.edu

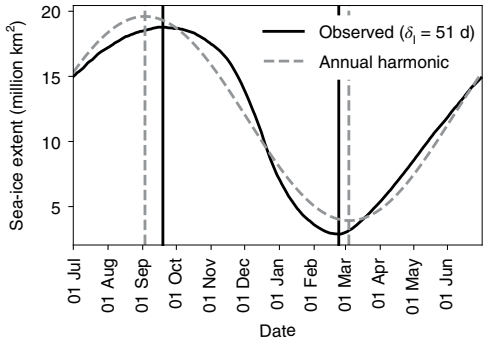

Fig. 1 | Observed mean seasonal cycle in Antarctic sea-ice extent averaged over 1979–1998. The annual harmonic (dashed curve), defined as the sum of the mean and the first Fourier component, is included to illustrate how the ice extent departs from a sinusoid. Vertical lines mark the maxima and minima of both curves. The seasonal asymmetry (δ_i) is indicated. The horizontal axis is shifted from the calendar year to emphasize the period of ice retreat. Data is from ref. [21].

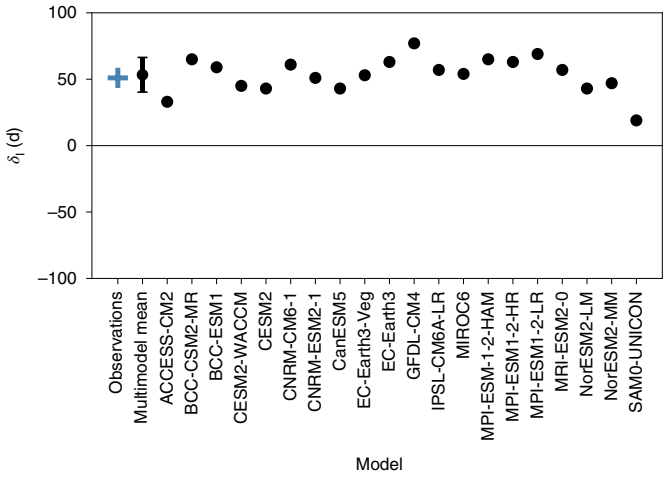

Fig. 2 | Antarctic sea-ice seasonal asymmetry (δ_i) in CMIP6 simulations and observations. The multimodel mean of the δ_i values is also indicated, with the error bar representing plus or minus one standard deviation among the models.

energy-balance model that includes a representation of sea-ice thermodynamics, simulating both latitudinal and seasonal variations. The model has no representation of land, and its spatial domain is a single hemisphere. The model simulates the evolution of the zonal-mean climate, which is represented using the enthalpy of the surface layer plus the atmospheric column:

$$E \equiv \begin{cases} -L\,h, & E < 0 \text{ (sea ice)} \\ c_w\,(T - T_f), & E \geq 0 \text{ (open water)} \end{cases}, \quad (1)$$

where L is the latent heat of fusion, h is sea-ice thickness, c_w is the heat capacity of the ocean mixed layer, T is the surface temperature and T_f is the freezing point. The specific heat capacity of the sea ice and the atmospheric column are both neglected. At each point in space, E evolves due to the net heating of the column, which includes top-of-atmosphere insolation S scaled by planetary co-albedo a; outgoing long-wave radiation, which is approximated as $A + B\,(T - T_f)$ with A and B constants; meridional heat transport, which is parameterized as diffusion $D\nabla^2 T$ with diffusivity constant D; and a constant heat input from the ocean F_b, such that

$$\frac{\partial E}{\partial t} = a\,S - [A + B\,(T - T_f)] + D\,\nabla^2 T + F_b. \quad (2)$$

When $E < 0$, equation (2) describes the evolution of sea-ice thickness h. In this case, the surface temperature that would balance the surface atmospheric energy flux with the vertical heat flux through ice, T_0, is calculated as

$$k\,\frac{T_f - T_0}{h} = -a\,S + [A + B\,(T - T_f)] - D\,\nabla^2 T, \quad (3)$$

where k is the thermal conductivity of the ice. The surface temperature takes this value if it is colder than the melting point, and otherwise surface melt occurs. Hence, the surface temperature is obtained as one of three possible cases,

$$T \equiv \begin{cases} T_f + E/c_w, & E \geq 0 \text{ (open water)} \\ T_f, & E < 0,\ T_0 > T_f \text{ (melting ice)} \\ T_0, & E < 0,\ T_0 < T_f \text{ (subfreezing ice)} \end{cases}. \quad (4)$$

The planetary co-albedo is given by

$$a \equiv \begin{cases} a_i, & E < 0 \text{ (sea ice)} \\ a_w, & E \geq 0 \text{ (open water)} \end{cases}, \quad (5)$$

where $a_w = a_0 - a_2 \sin^2\theta$, with θ the latitude and a_i, a_0 and a_2 constants. The top-of-atmosphere incident solar radiation in the Southern Hemisphere, S, is computed using present-day orbital parameters. We refer to this default insolation configuration as 'SHSol'. Further details regarding the model are provided in Methods.

In contrast with simplified variants of the model discussed below, we refer to this as the 'full' configuration of the idealized model. It qualitatively captures key characteristics of Southern Hemisphere seasonal and meridional variations in zonal-mean sea surface temperature[20], as well as the seasonal evolution of the zonal-mean ice edge latitude[21,22], as shown in Supplementary Fig. 5. The annual-mean ice edge approximately agrees with the observed value of 64.5° S (see Supplementary Fig. 5 for details), although the amplitude of the seasonal change in ice edge latitude is larger than observed. Importantly, the idealized model captures the observed asymmetry of the sea-ice seasonal cycle, with $\delta_i = 52$ days (black circle in second column of Fig. 3a).

Role of insolation in southern high latitudes

Next, we consider varied configurations of the idealized model to isolate what causes the asymmetry in the simulated sea-ice seasonal cycle. As a first simplification, we investigate what happens when the SHSol insolation field is replaced with the idealized sinusoidal insolation field from WE15 (which follows ref. [23]),

$$S(t, x) = s_0 - s_1\,\sin\theta\,\cos(\omega\,t) - s_2\,\sin^2\theta \quad (6)$$

with $\omega = 2\pi\,\mathrm{yr}^{-1}$ and s_0, and s_2 constants, which we refer to as 'IdealSol.' We find that with IdealSol insolation, there is approximately zero asymmetry in the idealized model (orange circle in second column of Fig. 3a; see also Supplementary Fig. 6), in contrast to the simulation with SHSol, which approximately matches the observed asymmetry. This implies that the top-of-atmosphere insolation is a key factor driving the asymmetry in the Antarctic sea-ice extent seasonal cycle.

Next, we consider further simplifications of the idealized model. In a variant denoted 'NoIce,' we remove the ice albedo feedback by

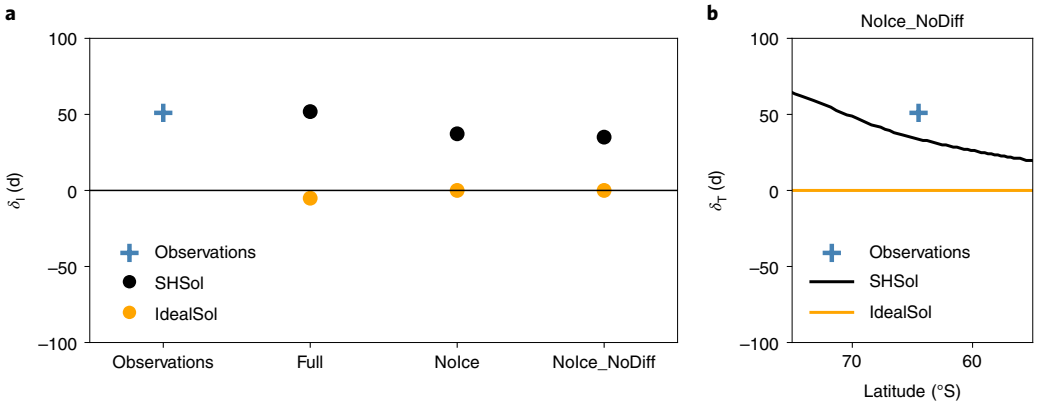

Fig. 3 | Antarctic sea-ice extent and temperature seasonal asymmetry in a range of configurations of the idealized climate model. a, Sea-ice extent asymmetry (δ_I) in model simulations using two choices for the solar forcing S and configurations with three levels of model complexity (horizontal labels), as well as in the observations. **b**, Asymmetry in the local temperature seasonal cycle δ_T as a function of latitude in the simplest model configuration (NoIce_NoDiff) using two choices for the solar forcing S; the observed value of δ_I is included at the observed annual-mean ice edge latitude for reference.

replacing equation (5) with $a = a_w$ at all locations, and we remove sea-ice thermodynamic effects by replacing equation (4) with $T = T_f + E/c_w$ regardless of the value of E. In this case, all effects of sea ice are omitted, and the model simulates an open ocean mixed layer at all locations regardless of the temperature. The sea-ice extent is still defined as the area polewards of the location where $E = 0$, which is equivalent in this configuration to $T = T_f$. We find that with SHSol insolation, the NoIce variant of the idealized model still captures much of the observed asymmetry, with $\delta_I = 37$ days (black circle in third column of Fig. 3a). As in the full configuration of the model, switching to IdealSol insolation removes the asymmetry (orange circle in third column of Fig. 3a).

To further simplify the idealized model, we next omit the diffusive horizontal heat transport by setting $D = 0$ in equation (2), in addition to the NoIce simplification described above. We refer to this configuration of the model as 'NoIce_NoDiff.' In this case, the model (1)–(5) reduces to a set of uncoupled ordinary differential equations that give independent solutions for $T(t)$ at each location:

$$c_w \frac{dT}{dt} = aS - [A + B(T - T_f)] + F_b. \quad (7)$$

We find that δ_I in the NoIce_NoDiff configuration ($\delta_I = 35$ days) agrees fairly closely with the NoIce configuration ($\delta_I = 37$ days) (Fig. 3a). This indicates that the role of meridional heat transport is not important in setting the seasonal asymmetry of the sea-ice extent.

Thus far, we have considered the times of maximum and minimum sea-ice extent, which is equivalent in the idealized model to the times of minimum and maximum ice edge latitude. Next, we turn to the seasonal cycle of temperature at a given latitude in the NoIce_NoDiff configuration, which can be more readily interpreted since each location is independent. We define δ_T as the difference in length between cooling and warming seasons, with positive values indicating a shorter warming season, analogous to the definition of δ_I for sea-ice extent. Figure 3b shows δ_T in the NoIce_NoDiff configuration using values of S and a associated with a range of latitudes. Using the IdealSol forcing, $\delta_T = 0$ at all latitudes. Using SHSol forcing, the values of δ_T are larger at more poleward locations. At the location of the observed annual-mean ice edge (64.5° S), the SHSol value is $\delta_T = 34$ days (Fig. 3b), which agrees closely with the ice extent asymmetry in this model configuration, $\delta_I = 35$ days (Fig. 3a). Consistent with this idealized model result, the observed seasonal cycle in surface temperature over much of the Southern Ocean and Antarctic continent is characterized by a warming period that is shorter than the cooling period[24].

Taken together, the results shown in Fig. 3a,b suggest that the seasonal asymmetry in sea-ice extent (δ_I) in the full configuration of the idealized model occurs for largely the same reasons as the seasonal asymmetry in temperature (δ_T) near 64.5° S in the NoIce_NoDiff configuration. Hence, we next interpret the relationship between T and S in equation (7) under SHSol forcing associated with 64.5° S.

We define the annual harmonic of insolation S_1 as the sum of the mean and the first Fourier component of S. In other words, S_1 is a sinusoidal fit to S. At 64.5° S, the annual harmonic S_1 varies between −35 and 468 W m^{-2}, and by definition its seasonal variations are exactly symmetric (Fig. 4a). Compared with S_1, S has a summer peak that is taller and narrower in shape, and it is flat at zero during polar night.

In Fig. 4c, the solution $T_1(t)$ to equation (7) under forcing $S_1(t)$ is plotted, along with the solution $T(t)$ under the forcing $S(t)$. Since S_1 is sinusoidal, T_1 is similar to the solution under IdealSol forcing, and it is a sinusoid with zero asymmetry. The seasonal cycle of T, by contrast, is asymmetric, with a warming season that is 34 days shorter than the cooling season (Fig. 4c; note that this is equivalent to the asymmetry associated with 64.5° S in Fig. 3b).

The forcing S departs from S_1 by having ~~more~~ less insolation near the temperature minimum and maximum and ~~less~~ more insolation during the periods of fastest warming and cooling (Fig. 4b). Therefore, the positive anomaly in insolation from November through January leads to faster warming, and the positive anomaly from May through July leads to slower cooling. Similarly, the negative anomaly from August through October leads to a delay in the onset of warming, whereas the negative anomaly from February through April leads to an earlier onset of cooling. This provides an intuitive physical explanation of why the period of warming and sea-ice retreat should be expected to be shorter than the period of cooling and ice advance given the insolation at southern high latitudes.

This explanation can be described more mathematically by noting that on seasonal timescales, the rate of change of temperature in equation (7) is approximately proportional to the departure of S from its annual-mean value (see Supplementary Text 1 for mathematical details). Hence, the relatively brief and intense mid-summer insolation peak causes a relatively rapid summer warming (and sea-ice retreat), followed by a more gradual winter cooling (and sea-ice growth). This can be seen more clearly by considering a cartoon insolation field with an exaggerated long polar night and brief and intense mid-summer insolation peak (Supplementary Fig. 7).

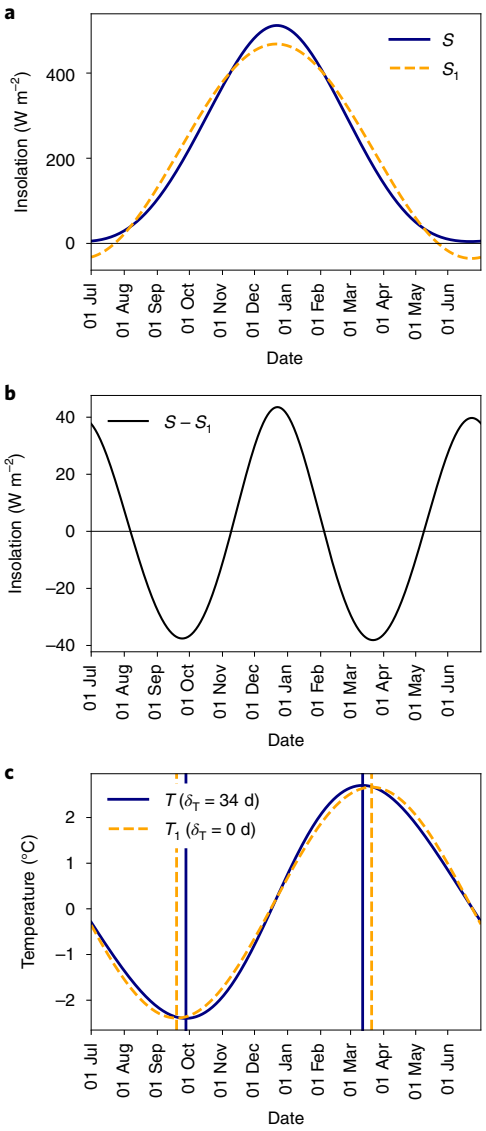

Fig. 4 | Insolation and resulting surface temperature in the simplest model configuration (NoIce_NoDiff). a, Top-of-atmosphere insolation at 64.5° S (S) and its annual harmonic (S_1). **b**, The difference between the two curves in panel **a**. **c**, Solutions (T and T_1) of the NoIce_NoDiff model configuration (equation (7)) under insolation forcings S and S_1.

Hemispheric contrasts

The seasonal asymmetry in the observed Arctic sea-ice extent is considerably smaller and opposite compared with the Antarctic, with the Arctic sea-ice advance season being shorter than the retreat season: $\delta_I = -25$ days in the Arctic, compared with $\delta_I = 51$ days in the Antarctic (Supplementary Fig. 1). In the CMIP6 models, there is more intermodel spread and less close agreement with the observations in the Arctic compared with the Antarctic (Supplementary Fig. 3a,b). The asymmetry in the CMIP6 multimodel mean is $\delta_I = 9 \pm 18$ days, of opposite sign to but marginally consistent with the observed value (the observations fall 1.9 standard deviations from the multimodel mean in Supplementary Fig. 3b). There is broadly similar behaviour in CMIP5 (Supplementary Fig. 3d) and CMIP3 (Supplementary Fig. 4b).

The insolation fields in the high latitudes of both hemispheres depart similarly from their annual harmonics, although due to Earth's current orbital parameters, the amplitude of this departure is somewhat smaller in the Northern Hemisphere (Supplementary Fig. 8). As a result, forcing the full configuration of the idealized model with top-of-atmosphere incident solar radiation in the Northern Hemisphere leads to a simulated seasonal asymmetry that is similar to but slightly smaller than the SHSol result: $\delta_I = 43$ days under Northern Hemisphere forcing compared with $\delta_I = 52$ days under Southern Hemisphere forcing (Supplementary Fig. 6). Similarly, the NoIce_NoDiff configuration of the model simulates an asymmetry of $\delta_T = 20$ days at 64.5° N, compared with $\delta_T = 34$ days at 64.5°S.

Previous research has taken the perspective that the nearly symmetric sea-ice seasonal cycle in the Arctic is expected and the asymmetric sea-ice seasonal cycle in the Antarctic is enigmatic. However, the intuitive physical explanation proposed here for the rapid seasonal sea-ice retreat in the Antarctic would be expected to apply similarly in the Arctic. This suggests that the enigma that remains to be explained is why the observed seasonal cycle in the Arctic sea-ice extent is not similarly asymmetric as in the Antarctic. Given that CMIP model biases in sea-ice asymmetry for the Arctic tend to be larger than for the Antarctic, the underlying mechanisms in the Arctic may be more subtle and difficult to capture in models.

In summary, the results of this study suggest that the observed seasonal asymmetry in Antarctic sea-ice extent arises directly from the deviation from a sinusoid of the seasonal cycle in high-latitude insolation. The brief and intense summer peak in high-latitude insolation causes rapid sea-ice retreat, whereas the long winter period with insolation at or near zero causes more gradual sea-ice growth. This relatively simple explanation is markedly different from those proposed in previous studies.

These findings draw on the results of a hierarchy of idealized climate models, and it should be noted that other processes not investigated here may also play a role, including zonal variations, the presence of landmasses and variations in mixed layer depth. Furthermore, seasonal variations in cloudiness may influence the impact of insolation on the sea-ice cover. Nonetheless, our results suggest that the seasonal distribution of top-of-atmosphere insolation in southern high latitudes is a primary driver of the observed asymmetry in the seasonal cycle of Antarctic sea-ice extent.

Online content

Any methods, additional references, Nature Research reporting summaries, source data, extended data, supplementary information, acknowledgements, peer review information; details of author contributions and competing interests; and statements of data and code availability are available at https://doi.org/10.1038/s41561-022-00913-6.

Received: 3 June 2021; Accepted: 17 February 2022;
Published online: 28 March 2022

References

1. Pellichero, V., Sallée, J.-B., Chapman, C. C. & Downes, S. M. The Southern Ocean meridional overturning in the sea-ice sector is driven by freshwater fluxes. *Nat. Commun.* **9**, 1789 (2018).
2. Orsi, A. H., Johnson, G. C. & Bullister, J. L. Circulation, mixing, and production of Antarctic Bottom Water. *Prog. Oceanogr.* **43**, 55–109 (1999).
3. Massom, R. A. et al. Antarctic ice shelf disintegration triggered by sea ice loss and ocean swell. *Nature* **558**, 383–389 (2018).
4. Arrigo, K. R., Worthen, D. L., Lizotte, M. P., Dixon, P. & Dieckmann, G. Primary production in Antarctic sea ice. *Science* **276**, 394–397 (1997).
5. Eayrs, C. et al. Understanding the seasonal cycle of Antarctic sea ice extent in the context of longer-term variability. *Rev. Geophys.* **57**, 1037–1064 (2019).
6. Gordon, A. L. Seasonality of Southern Ocean sea ice. *J. Geophys. Res.* **86**, 4193–4197 (1981).
7. Peixoto, J. P. & Oort, A. H. *Physics of Climate* (American Institute of Physics, 1992).
8. Enomoto, H. & Ohmura, A. The influences of atmospheric half-yearly cycle on the sea ice extent in the Antarctic. *J. Geophys. Res.* **95**, 9497–9511 (1990).
9. Stammerjohn, S. E., Drinkwater, M. R., Smith, R. C. & Liu, X. Ice–atmosphere interactions during sea-ice advance and retreat in the western Antarctic Peninsula region. *J. Geophys. Res. Oceans* **108**, 3329 (2003).

10. Cerrone, D., Fusco, G., Simmonds, I., Aulicino, G. & Budillon, G. Dominant covarying climate signals in the Southern Ocean and Antarctic sea ice influence during the last three decades. *J. Clim.* **30**, 3055–3072 (2017).
11. Eayrs, C., Faller, D. & Holland, D. M. Mechanisms driving the asymmetric seasonal cycle of Antarctic sea ice in the CESM Large Ensemble. *Ann. Glaciol.* **61**, 171–180 (2020).
12. Raphael, M. N., Handcock, M. S., Holland, M. M. & Landrum, L. L. An assessment of the temporal variability in the annual cycle of daily Antarctic sea ice in the NCAR Community Earth System Model, Version 2: a comparison of the historical runs with observations. *J. Geophys. Res. Oceans* **125**, e2020JC016459 (2020).
13. Turner, J. et al. An initial assessment of Antarctic sea ice extent in the CMIP5 models. *J. Clim.* **26**, 1473–1484 (2013).
14. Zunz, V., Goosse, H. & Massonnet, F. How does internal variability influence the ability of CMIP5 models to reproduce the recent trend in Southern Ocean sea ice extent? *Cryosphere* **7**, 451–468 (2013).
15. Shu, Q., Song, Z. & Qiao, F. Assessment of sea ice simulations in the CMIP5 models. *Cryosphere* **9**, 399–409 (2015).
16. Roach, L. A., Dean, S. M. & Renwick, J. A. Consistent biases in Antarctic sea ice concentration simulated by climate models. *Cryosphere* **12**, 365–383 (2018).
17. Roach, L. A. et al. Antarctic sea ice area in CMIP6. *Geophys. Res. Lett.* **47**, e2019GL086729 (2020).
18. Shu, Q. et al. Assessment of sea ice extent in CMIP6 with comparison to observations and CMIP5. *Geophys. Res. Lett.* **47**, GL087965 (2020).
19. Wagner, T. J. W. & Eisenman, I. How climate model complexity influences sea ice stability. *J. Clim.* **28**, 3998–4014 (2015).
20. Reynolds, R. W., Rayner, N. A., Smith, T. M., Stokes, D. C. & Wang, W. An improved in situ and satellite SST analysis for climate. *J. Clim.* **15**, 1609–1625 (2002).
21. Meier, W., Fetterer, F., Windnagel, A. & Stewart, J. *NOAA/NSIDC Climate Data Record of Passive Microwave Sea Ice Concentration Version 4* (NSIDC, 2021).
22. Eisenman, I., Schneider, T., Battisti, D. S. & Bitz, C. M. Consistent changes in the sea ice seasonal cycle in response to global warming. *J. Clim.* **24**, 5325–5335 (2011).
23. North, G. R. & Coakley, J. A. Differences between seasonal and mean annual energy-balance model calculations of climate and climate sensitivity. *J. Atmos. Sci.* **36**, 1189–1204 (1979).
24. Donohoe, A., Dawson, E., McMurdie, L., Battisti, D. S. & Rhines, A. Seasonal asymmetries in the lag between insolation and surface temperature. *J. Clim.* **33**, 3921–3945 (2020).

Methods

Observations. Sea-ice extent is defined as the area of grid cells with more than 15% sea-ice concentration, and we compute it using the National Snow and Ice Data Center Climate Data Record v.4 satellite sea-ice concentration dataset[21], with missing values filled using linear interpolation in time. Ice extent is the primary measure of the observed ice cover used by the National Snow and Ice Data Center because it is less sensitive than ice area to the misidentification of surface melt ponds, and hence we focus on the observed ice extent rather than ice area. We show the seasonal asymmetry in ice area for comparison in Supplementary Fig. 1b,c. For consistency across observations and models, we compute δ_l from the mean seasonal cycle of daily values averaged over the first 20 years of the satellite era (1979–1998). Data during leap years is linearly interpolated onto a 365-day year in the calculation of the mean seasonal cycle.

Comprehensive climate models. We use daily sea-ice area computed by ref. [25] for CMIP6 historical simulations and by ref. [16] for CMIP5 historical simulations, with the addition of Geophysical Fluid Dynamics Laboratory CM4 output in the present analysis of CMIP6 historical simulations. To illustrate how sensitive δ_l is to internal variability, we also include daily sea-ice area from the Community Earth System Model Large Ensemble (CESM1-LENS) (ref. [26]) computed by ref. [25]. The 35 members of CESM1-LENS differ only in atmospheric initial conditions in 1920 and thereby sample the range of internal climate variability simulated by CESM1. For CMIP3 historical simulations, which end in year 2000, we use monthly sea-ice area computed by ref. [27]. We focus on ice area in the CMIP analysis because the nonlinearity of the ice extent metric can cause artefacts regarding the spatial and the temporal evolution of simulated sea ice, and hence ice area has been adopted as the preferred measure in previous CMIP6 sea-ice analyses[28]. Nonetheless, for completeness, we include the asymmetry in the mean seasonal cycle of simulated sea-ice extent in the CMIP6 and CMIP5 models (Supplementary Fig. 10), as well as the CMIP3 models (Supplementary Fig. 11). We compute the mean 1979–1998 seasonal cycle in the CMIP6 and CMIP3 models, as in the observations, linearly interpolating daily values in leap years onto a 365-day year. On the basis of available processed output, we use the mean during 1980–1998 in the CMIP5 models. Next, we identify the dates of minimum and maximum ice area in the mean seasonal cycle in each model. For simulations that become ice-free during summer, we take the midpoint of the period with values below 0.1 million km^2 as the date of minimum ice area.

Idealized climate model and simplified variants. The full configuration of the idealized model is equivalent to the model introduced in WE15 except for the following changes. WE15 focused on the Northern Hemisphere and did not attempt to capture the detailed structure of the seasonal cycle. Hence, here we use realistic Southern Hemisphere insolation computed using code from ref. [29], whereas WE15 used the idealized sinusoidal form for S given in equation (6), and we use parameter values $A = 194.8\,\mathrm{W\,m^{-2}}$, $D = 0.625\,\mathrm{W\,m^{-2}\,K^{-1}}$ and $F_b = 5\,\mathrm{W\,m^{-2}}$ to better capture the seasonal cycle of Antarctic sea ice. Although we retain the value of c_w from WE15 (representing an ocean mixed layer depth of 75 m), we examined the impact of varying it, which we found left the results qualitatively unchanged although the quantitative value of δ_l becomes larger for larger values of c_w (Supplementary Fig. 9). Note that as in WE15, we use a value of F_b that is representative of the high-latitude ocean, which helps to accurately simulate the sea-ice evolution, but an artefact of the simple treatment of F_b is that the ocean becomes a weak global heat source. All other parameters are as in WE15, and a complete list of parameters is given in Supplementary Table 1. We solve the model (1)–(5) using the numerical method described in WE15.

We run each simulation for 100 years using 1,000 time steps per year and analyse the mean climatology over the last 20 years. We use a spatial resolution of 400 grid boxes between the Equator and the pole. The simulated ice extent is the area with $E < 0$. We compute this at each time step by linearly interpolating in the meridional coordinate x to determine the location associated with $E = 0$ and then calculating the area poleward of this location.

For each model configuration, we tune the parameter A, which controls the mean climate, such that the annual-mean ice edge latitude agrees with the observed value of 64.5° S. The values of A are listed in Supplementary Table 2.

The set of uncoupled ordinary differential equations that represent the NoIce_NoDiff model configuration (equation (7)) can be solved numerically by setting $D = 0$ in the NoIce configuration of the model code or approximately equivalently by analytically solving equation (7) for each Fourier component of the insolation field S.

Data availability

Data for the processed observations, comprehensive climate model output and idealized model results is available at https://doi.org/10.5281/zenodo.5913959.

Code availability

Code for the idealized climate model is available at https://doi.org/10.5281/zenodo.5913959 and https://eisenman-group.github.io.

References

25. Blanchard-Wrigglesworth, E., Donohoe, A., Roach, L. A., DuVivier, A. & Bitz, C. M. High-frequency sea ice variability in observations and models. *Geophys. Res. Lett.* **48**, e2020GL092356 (2021).
26. Kay, J. E. et al. The Community Earth System Model (CESM) Large Ensemble project: a community resource for studying climate change in the presence of internal climate variability. *Bull. Am. Meteorol. Soc.* **96**, 1333–1349 (2015).
27. SIMIP Community Arctic sea ice in CMIP6. *Geophys. Res. Lett.* **47**, e2019GL086749 (2020).
28. Notz, D. et al. The CMIP6 Sea-Ice Model Intercomparison Project (SIMIP): understanding sea ice through climate-model simulations. *Geosci. Model Dev.* **9**, 3427–3446 (2016).
29. Huybers, P. & Eisenman, I. *Integrated Summer Insolation Calculations* IGBP PAGES/WDCA Contribution Series 2006-079 (NOAA/NCDC Paleoclimatology Program, 2006).

Acknowledgements

We thank C. Eayrs for helpful discussions. This work was supported by the Scientific Committee on Antarctic Research (SCAR) Fellowship Program; the National Oceanic and Atmospheric Administration (NOAA) Climate and Global Change Postdoctoral Fellowship Program, which is administered by UCAR's Cooperative Programs for the Advancement of Earth System Science (CPAESS) under award NA18NWS4620043B; US National Science Foundation grants OPP-1643445, OCE-2048590 and OPP-1643431; and NOAA grant NA18OAR4310274.

Author contributions

T.J.W.W. and L.A.R. conceived the study question. I.E., L.A.R. and T.J.W.W. designed the research, constructed the idealized models, interpreted the results and developed the conclusions. L.A.R. analysed the observations and CMIP output. C.M.B. and E.B.-W. assisted with initial attempts to address the question. L.A.R., I.E. and T.J.W.W. wrote the manuscript with contributions from all co-authors.

Competing interests

The authors declare no competing interests.

Additional information

Supplementary information The online version contains supplementary material available at https://doi.org/10.1038/s41561-022-00913-6.

Correspondence and requests for materials should be addressed to I. Eisenman.

Peer review information *Nature Geoscience* thanks Clare Eayrs, Kenneth Golden and the other, anonymous, reviewer(s) for their contribution to the peer review of this work. Primary Handling Editor: Tom Richardson, in collaboration with the *Nature Geoscience* team.

Reprints and permissions information is available at www.nature.com/reprints.

Supplementary Information for "Asymmetry in the seasonal cycle of Antarctic sea ice driven by insolation"

Roach, Eisenman, Wagner, Blanchard-Wrigglesworth and Bitz

Text S1: Mathematical analysis of NoIce_NoDiff model configuration

Equation (7) in the main text, which represents the NoIce_NoDiff configuration of the model, can be rewritten as

$$\frac{dT}{dt} = \frac{T_0 - T}{\tau} + \frac{a\,S'(t)}{c_w}, \tag{S1}$$

where $T_0 \equiv \frac{a\,s_0 - A + B\,T_f + F_b}{B}$ is the time average of the spun up model solution and $\tau \equiv \frac{c_w}{B}$ is the model response timescale. Here we have decomposed the forcing as $S = s_0 + S'(t)$, where s_0 is the annual mean and $S'(t) \equiv S - s_0$ is the time-varying departure.

Next we subtract the annual mean from both sides of Eq. (S1), which leads to

$$\frac{dT'}{dt} = -\frac{T'}{\tau} + \frac{a\,S'(t)}{c_w}, \tag{S2}$$

with $T' \equiv T - T_0$. Two asymptotic regimes of Eq. (S2) can be considered. If the timescale of variability of $S'(t)$ (and hence similarly of T') is a lot longer than τ, then $\frac{dT'}{dt} \ll \frac{T'}{\tau}$, and the dominant balance in Eq. (S2) is

$$0 \approx -\frac{T'}{\tau} + \frac{a\,S'(t)}{c_w}, \tag{S3}$$

so that the temperature is always in approximate steady-state with the forcing: $T' \approx \frac{a\,S'(t)\,\tau}{c_w} = \frac{a\,S'(t)}{B}$. On the other hand, if the timescale of variability of $S'(t)$ (and hence similarly of T') is a lot shorter than τ, then $\frac{dT'}{dt} \gg \frac{T}{\tau}$, and the dominant balance in Eq. (S2) is

$$\frac{dT'}{dt} \approx \frac{a\,S'(t)}{c_w}, \tag{S4}$$

so the temperature is always in approximate quadrature with the forcing.

Inserting the idealized model parameters, $\tau \equiv \frac{c_w}{B} = 4.7$ yrs. Meanwhile, $S'(t)$ is annually periodic, so its timescales of variation are shorter than 1 yr. Hence Eq. (S2) can be roughly approximated by the second asymptotic regime (S4), with the rate of change of T scaling with the anomaly of S from its annual-mean value. This implies that having a narrow summer insolation peak with $S > s_0$ and a wider winter insolation trough with $S < s_0$, as occurs in high latitudes, leads to a brief summer warming period and a longer winter cooling period.

Table S1 Default parameter values in the idealized climate model.

D	diffusivity for heat transport	0.625 $\mathrm{Wm^{-2}K^{-1}}$
A	outgoing longwave radiation when $T = T_f$	194.8 $\mathrm{Wm^{-2}}$
B	outgoing longwave radiation temperature dependence	2.1 $\mathrm{Wm^{-2}K^{-1}}$
c_w	ocean mixed layer heat capacity	9.8 $\mathrm{W\,yr\,m^{-2}K^{-1}}$
a_0	ice-free coalbedo at equator	0.7
a_2	ice-free coalbedo spatial dependence	0.1
a_i	coalbedo where there is sea ice	0.4
F_b	heat flux from ocean below	5 $\mathrm{Wm^{-2}}$
k	sea ice thermal conductivity	2 $\mathrm{Wm^{-1}K^{-1}}$
L_f	sea ice latent heat of fusion	9.5 $\mathrm{W\,yr\,m^{-3}}$
T_f	freezing point	0° C
s_0	IdealSol insolation at equator	420 $\mathrm{Wm^{-2}}$
s_1	IdealSol insolation seasonal dependence	338 $\mathrm{Wm^{-2}}$
s_2	IdealSol insolation spatial dependence	240 $\mathrm{Wm^{-2}}$

Table S2 Description of each idealized model simulation and values of the parameter A.

Configuration	Description	A for SHSol	A for IdealSol
Full	Default configuration	194.8 W $\mathrm{m^{-2}}$	195.0 W $\mathrm{m^{-2}}$
NoIce	Omitting ice albedo feedback and ice thermodynamic effects	201.6 W $\mathrm{m^{-2}}$	201.5 W $\mathrm{m^{-2}}$
NoIce_NoDiff	As in NoIce but also omitting horizontal heat transport	138.6 W $\mathrm{m^{-2}}$	143.6 W $\mathrm{m^{-2}}$

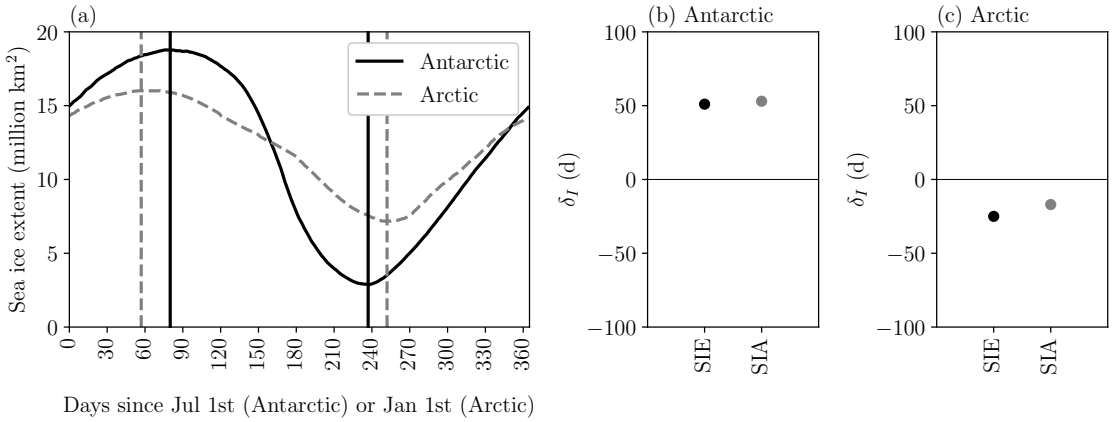

Fig. S1 Observed[21] 1979-1998 mean seasonal cycle of ice extent and ice area in both hemispheres. (a) As in Fig. 1 in the main text but for both the Arctic and the Antarctic. The time axis is shifted by half a year between the two curves to better align the times of maximum and minimum. (b) Seasonal asymmetry (δ_I) in Antarctic sea ice extent (SIE) and sea ice area (SIA). (c) As in panel (b) but for the Arctic.

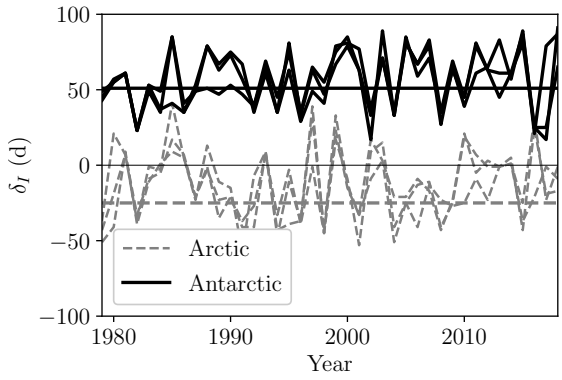

Fig. S2 Year-to-year variations in the value of δ_I in the Antarctic (solid) and Arctic (dashed) computed for each individual year during 1979-2018. For each hemisphere, three lines are plotted indicating the Climate Data Record (CDR), NASA Team, and Bootstrap sea ice datasets (all included with the CDR data release[21]). Horizontal lines show δ_I for the 1979-1998 mean seasonal cycle in the CDR dataset. The standard deviation of plotted year-to-year variability in the Antarctic CDR data is 18 days. When we compute the ice extent mean seasonal cycle averaged over each consecutive 20-year period during the entire 1979-2020 record, we find asymmetry values δ_I that vary between 49 and 79 days in the Antarctic and between −31 and 1 days in the Arctic.

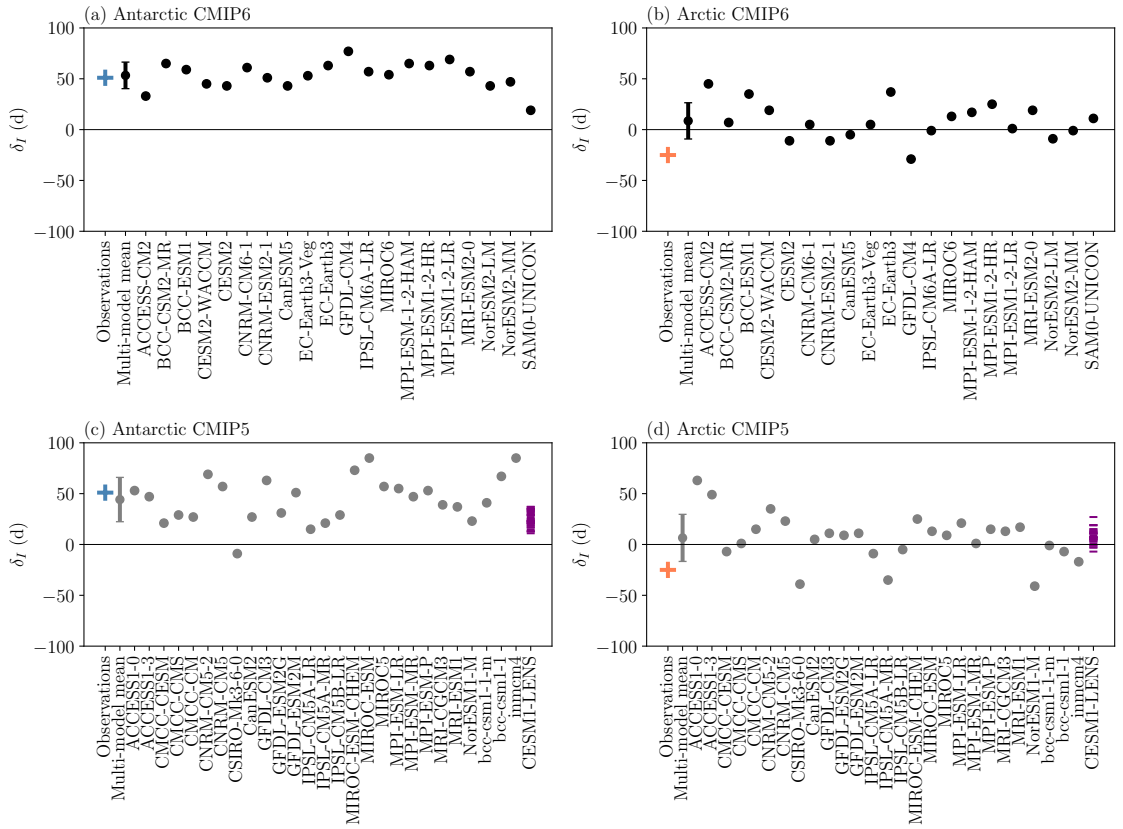

Fig. S3 Seasonal asymmetry (δ_I) in CMIP6 and CMIP5 simulations, as well as CESM1-LENS. (a) Equivalent to Fig. 2 in the main text. (b) As in panel (a) but for the Arctic. (c-d) As in panels (a-b) but for CMIP5 and CESM1-LENS.

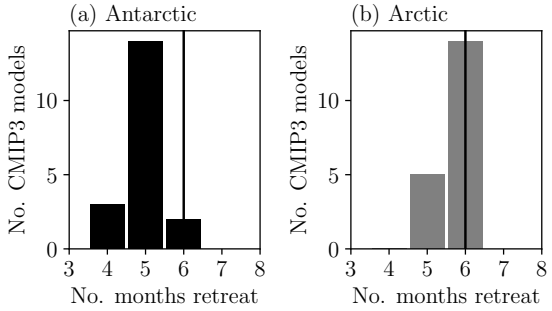

Fig. S4 Asymmetry in CMIP3 model results. (a) The number of months between the maximum and the minimum sea ice area in the simulated 1979-1998 mean seasonal cycle in 19 CMIP3 models. (b) As in panel (a) but for the Arctic.

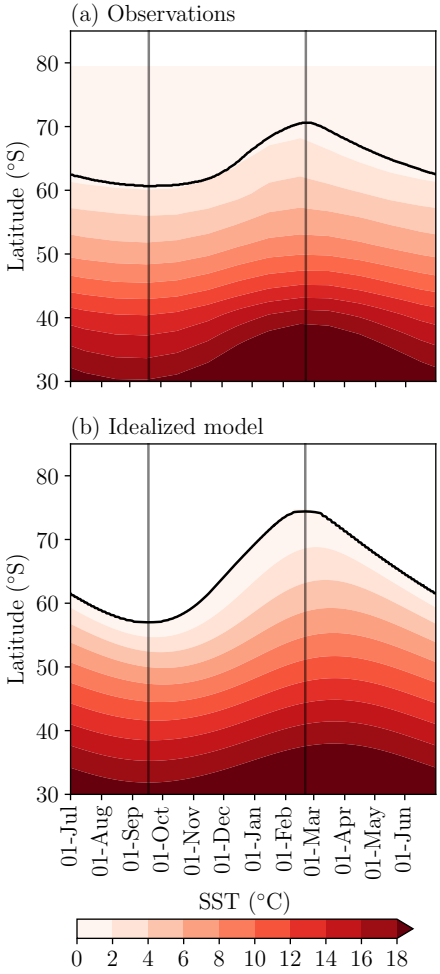

Fig. S5 Idealized model compared with observations. (a) Observed Southern Hemisphere sea surface temperature (colours) and zonal-mean ice edge latitude (black line). (b) As in panel (a) but using the simulation results from the Full configuration of the idealized model with SHSol forcing. Vertical lines indicate the times of maximum and minimum ice edge latitude, which correspond with the times of ice extent extrema. Here the observations are from the 1982-1998 mean annual cycle in NOAA OISSTv2 sea surface temperature[20] and NSIDC Climate Data Record sea ice extent[21], and the zonal-mean ice edge latitude is computed following ref 22 as the latitude with ocean area poleward of it equal to the ice extent, which is a quantity that maps monotonically from the ice extent. Note that evolution of the ice edge latitude in the idealized model broadly agrees with the observations, although the summer ice retreat in the model goes further poleward than the Antarctic continent permits in observations.

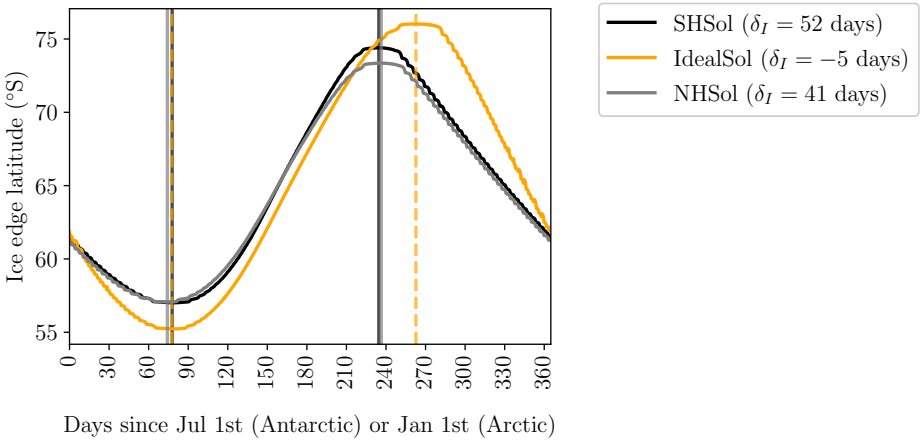

Fig. S6 Seasonal cycle in the ice edge latitude simulated with the Full configuration of the idealized model using IdealSol and SHSol insolation forcing, as well as Northern Hemisphere insolation forcing (indicated here as NHSol, using the same value of A as the SHSol run).

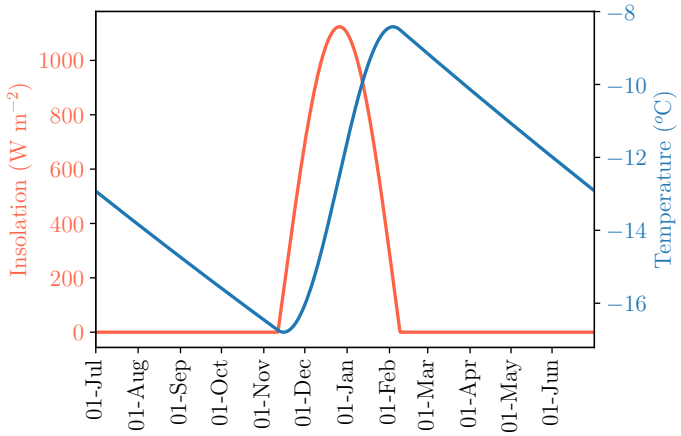

Fig. S7 Cartoon insolation field S and resulting temperature T simulated with Eq. (7) in the main text. Here the insolation field is constructed from the insolation at 90°S by making the period that is not polar night half as long and twice as bright in order to exaggerate the brevity of the mid-summer insolation peak, and the values of A and a are as in the SHSol case at 64.5°S. Note the extreme seasonal asymmetry in the temperature response, with a brief period of warming and a long period of cooling.

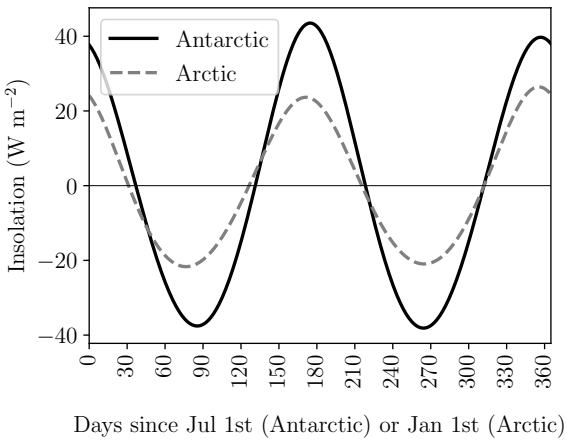

Fig. S8 As in Fig. 4b in the main text, but including the Arctic. This shows the difference between the top-of-atmosphere solar insolation and its annual harmonic ($S - S_1$) at 64.5° latitude in each hemisphere.

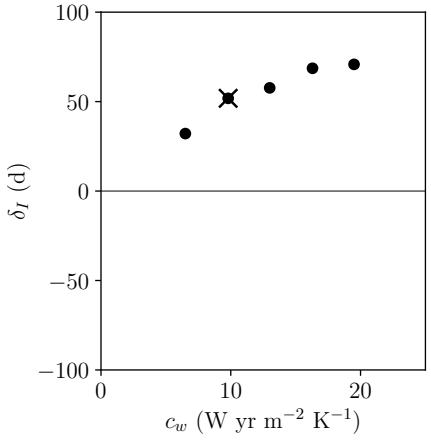

Fig. S9 Antarctic sea ice extent seasonal asymmetry in the Full version of the WE15 model with the ocean mixed layer heat capacity (c_w) varied between two thirds and double the default value (marked ×), which corresponds to a mixed layer depth of 75 m.

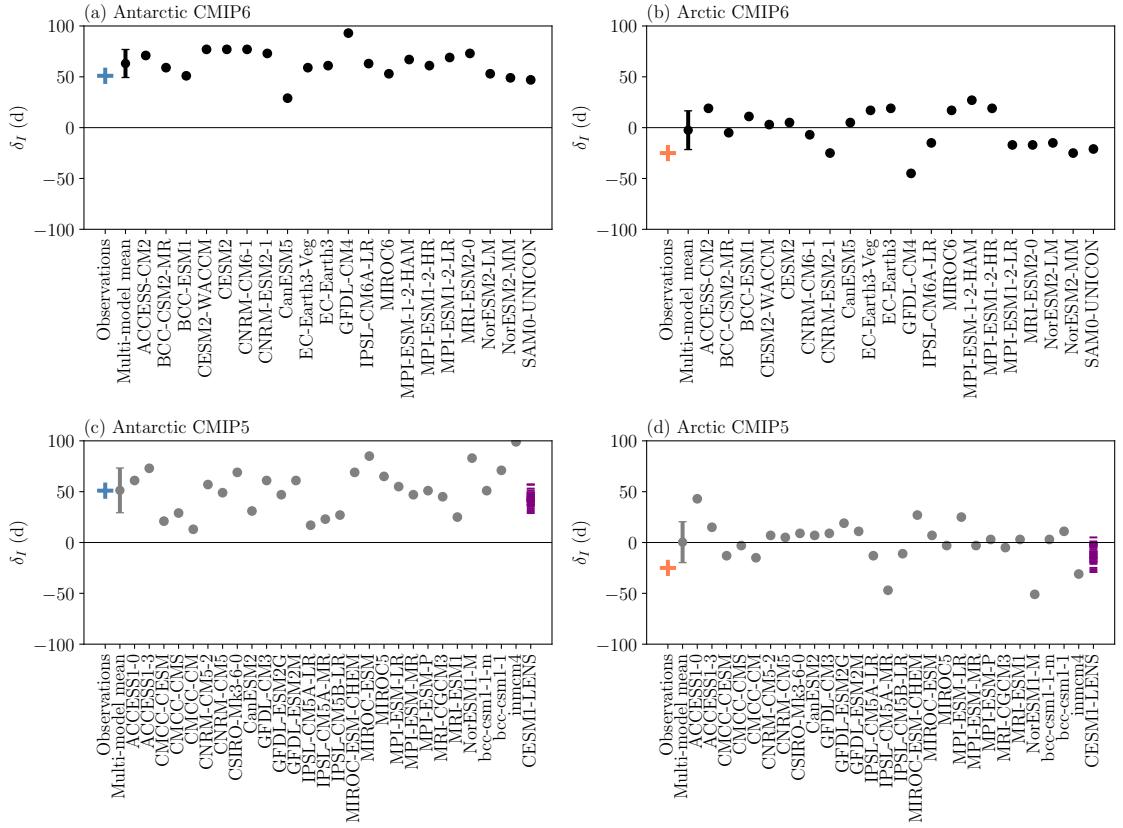

Fig. S10 As in Fig. S3, but using simulated ice extent rather than simulated ice area. Note that this figure and Fig. S3 both use the observed ice extent (see Methods).

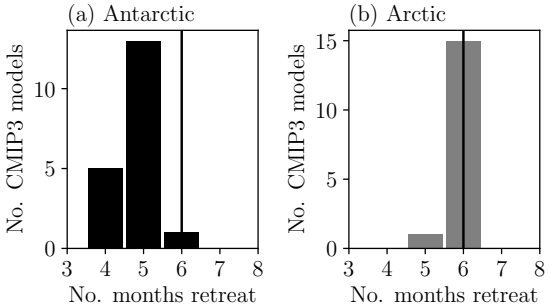

Fig. S11 As in Fig. S4, but using simulated ice extent rather than simulated ice area.